The first 40Ar–39Ar date from Oxfordian ammonite-calibrated volcanic layers (bentonites) as a tie-point for the Late Jurassic

The first $^{40}Ar/^{39}Ar$ age from Oxfordian ammonite-calibrated volcanic layers (bentonites) as a tie-point for the Late Jurassic

P. Pellenard[1*], S. Nomade[2], L. Martire[3], F. De Oliveira Ramalho[4], F. Monna[5], H. Guillou[2]

[1]*Biogéosciences, CNRS-UMR 6282, Université de Bourgogne, F-21000 Dijon, France*

[2]*LSCE-IPSL, CNRS-UMR 8212, CEA Orme, F-91191 Gif-sur-Yvette, France*

[3]*Dipartimento di Scienze della Terra, University of Torino, via Valperga Caluso 35 10125 Torino, Italy*

[4]*Statoil ASA, Grenseveien 21, 4313 Forus, Norway*

[5]*ARTeHIS, CNRS-UMR 6298, Université de Bourgogne, F-21000 Dijon, France*

* Tel.: + 33 380-39-63-66; Fax: +33 380-39-63-87; e-mail: Pierre.Pellenard@u-bourgogne.fr

Running head: A new tie-point for Late Jurassic calibration

ABSTRACT

Eight volcanic ash layers, linked to large explosive events caused by subduction-related volcanism from the Vardar Ocean back arc, interbedded with marine limestones and cherts, have been identified in the Rosso Ammonitico Veronese Formation (north-eastern Italy). The thickest ash layer, attributed to the *Gregoryceras transversarium* ammonite biozone (Oxfordian Stage), yields a precise and reliable $^{40}Ar/^{39}Ar$ age of 156.1 ± 0.89 Ma which is in

21 better agreement with the GTS2004 boundaries, than the current GTS2012. This first
22 biostratigraphically well-constrained Oxfordian age is proposed as a new radiometric tie-point
23 to improve the Geologic Time Scale for the Late Jurassic whose ammonite-bearing
24 radiometric ages are particularly scarce.

25 Keywords: geochronology, palaeovolcanism, bentonite, Oxfordian, Jurassic Time Scale

26 **1. INTRODUCTION**

27 There are no well-constrained direct radiometric dates, closely tied to ammonite
28 biostratigraphy currently available for the whole of the Upper Jurassic (Gradstein et al.,
29 2012). Some Upper Jurassic Ar-Ar dates are integrated as secondary guides in the GTS2012:
30 1) a suite of dates from the almost totally non-marine Morrison Fm in USA (Gradstein, Ogg
31 & Smith, 2004; Ogg, Ogg & Gradstein, 2008), 2) dates from Oxfordian tuffs intercalated in
32 terrestrial sediments in China (Chang et al. 2009), and 3) dates from ocean floor basalt veins
33 in the Pacific (Gradstein et al., 2012). A single Re/Os date is available from ammonite-
34 bearing marine sedimentary successions in the Lower Kimmeridgian (Selby, 2007). As a
35 consequence, the Late Jurassic Time Scale derives mainly from the Pacific seafloor spreading
36 numerical model of the M-sequence magnetic polarity pattern and from limited recent
37 cyclostratigraphic studies (Ogg & Smith 2004; Ogg et al., 2010; Gradstein et al., 2012).
38 Magnetostratigraphy can be calibrated with ammonite assemblage biochronology, which is
39 mainly defined in north-western European domains (Cariou & Hantzpergue 1997; Morton
40 2006). However, provincialism in Boreal, sub-Boreal, sub-Mediterranean and Tethyan
41 domains prevents unequivocal zonation correlation, especially for certain intervals and hence,
42 introduces a temporal bias in the magnetostratigraphic model. Despite recent progress in
43 reducing this bias (Ogg et al., 2010; Przybylski et al., 2010; Gradstein et al., 2012), the
44 scarcity of interbedded volcanic units in ammonite-bearing marine succession hinders the

accurate numerical calibration of the Late Jurassic Time Scale, even with the progress made in GTS2012, including improved numerical ages for stage boundaries obtained by selecting only single-zircon U-Pb ages, recalculating $^{40}Ar/^{39}Ar$ dates and more precise magnetostratigraphy and cyclostratigraphy.

Therefore, to obtain radiometrically calibrated tie-points for the Late Jurassic, biostratigraphically-constrained volcanic ash layers in Tethyan basins have been studied (Pellenard et al., 2003; Pellenard & Deconinck 2006). Here, we focus on eight volcanic ash layers, weathered into bentonites, sampled in pelagic cherty limestones from the Altopiano di Asiago (Trento Plateau domain, north-eastern Italy; Bernoulli & Peters 1970; Martire 1996). We present a new $^{40}Ar/^{39}Ar$ radiometric date from one of these bentonites providing the first radiometric tie-point from biostratigraphically well constrained sedimentary strata for the Middle Oxfordian and discuss volcanic events and potential sources.

2. MATERIAL AND METHOD

Six bentonite layers were identified by their field characteristics, mineralogy and geochemical features at the Serrada section and a further five, 28 km away, at the Echar and Kaberlaba sections, in the Altopiano di Asiago (Trentino Alto Adige and Veneto regions, Italy; Fig. 1a). Weathering of volcanic ashes into clays produced bentonite deposits during the early stages of diagenesis at the sediment/seawater interface. In the Rosso Ammonitico Veronese (RAV), bentonites appear as continuous centimetre-thick red or white plastic clay-rich horizons, interbedded with limestones and cherts (Figs. 1b and 3a). The RAV is an Upper Bajocian to Tithonian pelagic limestone succession, which can be divided into three units (Figs. 1b, 2a; Sarti, 1985; Martire, 1992; Martire et al., 2006). The lower unit (Rosso Ammonitico Inferiore: RAI) and the upper unit (Rosso Ammonitico Superiore: RAS) are composed of massive nodular limestones, while the Rosso Ammonitico middle unit (RAM), containing all the

bentonite layers, consists of thin, evenly bedded, non-nodular, chert-rich limestones. The RAM unit reaches a maximum thickness of 10 m although it occasionally thins out and disappears (Martire 1996; Fig. 2a).

Mineralogical (X-ray diffraction, Biogeosciences Dijon, France) and elemental (inductively coupled plasma-optical emission spectrometry [ICP-OES] and ICP-MS [MS, mass spectrometry], CRPG Nancy, France) analyses were performed on all powdered samples to confirm their volcanic nature (online Supplementary Material Table S1 available at http://journals.cambridge.org/geo). Principal Component Analysis (PCA) was used to evaluate the number of volcanic events. Prior to the correlation matrix-based PCA, trace element concentrations were re-expressed assuming an initial volcanic concentration of 15% Al_2O_3 (Spears et al., 1999; Pellenard et al., 2003). This procedure reduces variability in lithophile element concentration which could be owing to post-depositional diagenetic processes, such as dilution by authigenic phases, or concentration by dissolution of less stable minerals.

The $^{40}Ar/^{39}Ar$ dating (OSIRIS reactor CEA Saclay, France) was performed by step-heating about 30 small (<100 µm) transparent sanidines, carefully handpicked under a binocular microscope after several treatments from the Kaberlaba section AB4 bentonite (original sample weight 2 kg, see online Supplementary Material available at http://journals.cambridge.org/geofor details). Each Ar isotope measurement consists of 20 cycles by peak switching between the different argon isotopes. The J value was determined using three single ACs (Alder Creek sanidine) grains taken from the same hole as the sample. Recently, Renne et al. (2010, 2011) published an optimisation model for estimating the partial decay constants of ^{40}K and $^{40}Ar^*/^{40}K$ ratio of FCs (Fish Canyon sanidine). This calibration reduces systematic uncertainties in the $^{40}Ar/^{39}Ar$ system from *ca.* 2.5% (Steiger & Jäger, 1977) to 0.27%. The optimisation model yields an age for ACs of 1.2056 Ma, equivalent to

FCs of 28.294 Ma, that overlaps at the 2σ confidence level the astronomically tuned ACs and FCs ages reported by Kuiper et al. (2008). The optimisation model of Renne et al. (2010, 2011) used pairs of $^{238}U/^{206}Pb$ and $^{40}Ar/^{39}Ar$ data as inputs. Therefore, $^{40}Ar/^{39}Ar$ ages calibrated with this optimisation model could be directly compared to U/Pb. The corresponding J value (0.0006846 ± 0.00000137, 1σ) was calculated using the Renne et al., (2011) calibration of ACs. The J uncertainty corresponds to the standard deviation of the weighted mean of three ACs single grains (see Nomade et al., 2010, 2011 and Supplementary Material available at http://journals.cambridge.org/geo for detailed methodology).

3. BIOSTRATIGRAPHY AND CORRELATION OF ASH LAYERS

At Kaberlaba, calcareous nannofossil assemblages indicate a Late Callovian age for the base of the RAM unit, while the following ammonite assemblage: *Gregoryceras fouquei, Passendorferia (Enayites) birmensdorfensis, Passendorferia* cf. *ziegleri, Perisphinctes (Otosphinctes) nectobrigensis, Perisphinctes (Dichotomosphinctes)* aff. *elisabethae, Sequeirosia (Gemmellarites)* aff. *trichoplocus, Subdiscosphinctes richei,* which is characteristic of the *Gregoryceras transversarium* Biozone, indicates a Middle Oxfordian age for the top of the RAM unit (Clari, Martire & Pavia., 1990; Martire 1992; 1996; Martire et al., 2006, see Fig. S1 in Supplementary Material available at http://journals.cambridge.org/geo for photographs of typical ammonites *of the G. transversarium* Biozone). All these ammonite taxa come from the bed between bentonites AB3 and AB4 at Kaberlaba, where preservation is better than in the rest of the section. They are all exclusive to the *G. transversarium* Biozone, except for *G. fouquei,* which spans the *G. transversarium* Biozone and the overlying *Perisphinctes (Dichotomoceras) bifurcatus* Biozone. The overlying RAS unit contains ammonites such as *Orthosphinctes (Ardescia)* gr. *inconditus, Crussoliceras aceroides* and *Idoceras (Lessiniceras)* sp., characteristic of the *Taramelliceras strombecki* and *Presimoceras*

herbichi biozones of the Lower Kimmeridgian (Sarti, 1993; Clari, Martire & Pavia., 1990; Martire, 1992, 1996). Therefore, at Kaberlaba, there is a major hiatus (four ammonite biozones) between the upper part of the Middle Oxfordian and the lowermost part of the Lower Kimmeridgian (Fig. 2a). However, the RAM unit of the Echar section provides a biostratigraphic framework for bentonites AB4 and AB5 as here the overlying sediments are well dated, with no hiatus. The RAM unit at Echar contains the same five bentonites and is overlain by three stromatolitic beds, the first of which belongs to the *G. transversarium* Biozone, with the same taxa as Kaberlaba. The second stromatolitic bed is dated to the Lower Kimmeridgian (*Sowerbyceras silenum* Biozone), on the basis of the following assemblage: *Taramelliceras* cf. *rigidum, Idoceras (Lessniceras)* cf. *raschii, Lithacosphinctes* cf. *stromeri, Mesosimoceras evolutum, Euaspidoceras (Epaspidoceras)* sp. The third stromatolitic bed belongs to the *P. herbichi* Biozone (Lower Kimmeridgian, Fig. 2a). In the Serrada section, the RAM unit extends from the Upper Callovian to the Middle Oxfordian (G. *transversarium* Biozone). As all bentonites sampled were from the RAM unit, they therefore date from the Upper Callovian to the Middle Oxfordian. As ammonites diagnostic of the *G. transversarium* Biozone were found just below AB4 at Kaberlaba and just above at Echar, the two uppermost bentonite beds in these sections (AB4 and AB5), easily recognisable because of their thickness and vivid red colour (Fig. 3a), are attributed to the *G. transversarium* Biozone (Fig.2a).

The bentonites studied, which correspond to pure-smectite horizons containing occasional volcanic crystals (e.g. sanidine, quartz, biotite) are marked by positive anomalies in Th, Ta, Hf and Ga, which is characteristic of bentonite deposits (Spears et al., 1999; Pellenard et al., 2003, Table S1 in online Supplementary Material available at http://journals.cambridge.org/

141 geo). Principal Component Analysis (PCA) was used to examine possible similarities between
142 ash layers in the Serrada and Kaberlaba sections, 28 km apart, in order to correlate the
143 bentonites and to evaluate the number of volcanic events and their preservation in the Trento
144 Plateau domain. The most typically immobile, volcanogenic elements were selected for this
145 analysis: Hf, Ga, Th, Ta, La, Zr and Ti (Fig. 2b). In the F2 *vs* F1 diagram (Fig. 2b),
146 representing more than 80% of the total variance, four groups consistent with the stratigraphy
147 can be clearly identified: (*i*) AB2, AB3, (*ii*) SB1, SB2, AB1, (*iii*) SB3, AB4, and (*iv*) SB4,
148 SB5, SB6, AB5. The first Kaberlaba level, AB1, corresponds either to the first Serrada level
149 SB1 or possibly to SB2. Samples AB2 and AB3 (Kaberlaba) have no equivalent in the
150 Serrada section, indicating that these events were not systematically preserved. Sample AB4,
151 a thick red bentonite from Kaberlaba, is geochemically similar to SB3, the thickest bentonite
152 from Serrada. Sample AB5 from Kaberlaba probably corresponds to SB4, perhaps to SB5 or
153 SB6. At least eight individual volcanic events are therefore identified using PCA (Fig. 2b),
154 with correlations over a large geographic area, coherent with the biostratigraphic framework.

155 **4. ^{40}AR/^{39}AR RESULTS**

156
157 We used the laser-fusion step-heating $^{40}Ar/^{39}Ar$ method to date level AB4, which contains the
158 highest abundance of well-preserved sanidines and which is also biostratigraphically the most
159 precisely constrained. The apparent age spectrum obtained for the AB4 sanidines is 100%
160 concordant (Fig 3b, details in Supplementary Material Tables S2 and S3 available at
161 http://journals.cambridge.org/geo): all steps yield indistinguishable ages, with a well-defined
162 plateau age of 156.1 ± 0.89 Ma (2σ full uncertainty propagation). As the inverse isochron
163 displays low scatter because of its highly radiogenic content, it was not used, given the
164 imprecise initial atmospheric $^{40}Ar/^{36}Ar$ ratio obtained. The plateau age we obtain can be
165 directly compared to U–Pb ages available for the Jurassic Time Scale (GTS2004, GTS2012

and Pálfy, 2008). We however present alternative calculations (Table 1) using several standards (Nomade et al., 2005; Kuiper et al., 2008) and total ^{40}K decay constants (Steiger & Jäger 1977; Renne et al., 2011) since the Mesozoic GSSP time scale (GTS2004 and GTS2012) was based on many ^{40}Ar-^{39}Ar ages, using different ^{40}K constant and various standards. The full uncertainty propagation of the Steiger & Jäger (1977) ^{40}K total decay constant (*ca.* 2.5% at 2σ) results in an AB4 error of about 4.0 Ma, while the Min et al., (2000) ^{40}K decay constant, proposed by Kuiper et al., (2008), could not be retained because of its high degree of uncertainty of 3.9% at 2σ, compared to the 0.27% from Renne et al., (2010, 2011) that has been adopted in this study.

5. NATURE AND SOURCE OF VOLCANIC EVENTS

The bentonite profile in the MORB-normalised multi-element plot clearly shows that the initial ash layers result from an evolved calc-alkaline magma (Fig. 3c and online Supplementary Material Fig. S2 available at http://journals.cambridge.org/geo). The characteristic Nb depletion and the Hf-Th-Ta diagram are typical of subduction-related arc materials, while the Zr/TiO_2 *vs* Nb/Y diagram indicates mainly andesite to rhyodacite products (online Supplementary Material Fig. S2 available at http://journals.cambridge.org/geo). As no lavas or thick pyroclastic deposits have been identified in or nearby the Trento domain within the Upper Jurassic (Bernoulli & Peters 1970; Pellenard et al., 2003), sources must be distant. In addition, fine-grained ashes emitted by highly explosive eruptions are known to be distributed over long distances (>1000 km). This hypothesis is supported by (*i*) the correlation indicated by the PCA of several events with similar features (e.g. thickness), over a large area in the Venetian Pre-Alps, and (*ii*) the size (50-100 µm) of the preserved pyroclastic minerals (i.e. sanidine and quartz). Emissions of tholeiitic basalts, andesites and pyroclastites are reported for the Middle-Late Jurassic from

190 the island-arc magmatism in the eastern Rhodope-Thrace region in Bulgaria and Greece
191 (Bonev & Stampfli 2008). This volcanism was associated with the southward subduction of
192 the Meliata-Maliac Ocean under the supra-subduction back-arc Vardar Ocean/island-arc
193 system (Bonev & Stampfli 2008). The Vardar geodynamic context undoubtedly produced
194 huge eruptions and subsequent widespread ashes. The age of the Vardar subduction, ranging
195 from the Early Jurassic incipient proto-arc to the Middle-Late Jurassic arc-back arc spreading,
196 is coherent with the biostratigraphic age of the bentonites studied here, whose geochemical
197 fingerprint is similar to that of the Vardar pyroclastics (Fig. 3c). This evidence supports
198 Vardar island-arc volcanism as the probable source of the ash layers found in the Venetian
199 Pre-Alps.

200 **6. A NEW TIE-POINT FOR THE LATE JURASSIC TIME SCALE**

201 Among the few direct radioisotopically and

202 There are few biostratigraphically well-constrained radiometric tie-points for the Middle-Late
203 Jurassic. Fot eh Middle Jurassic, the only available U-Pb ages are from (i) British Columbia
204 bentonites, ascribed to the early Late Bathonian (Pálfy, 2008), and (ii) an ash layer (164.6 ±
205 0.2 Ma) in the Neuquén province (Argentina), at the Bathonian-Callovian boundary (Kamo &
206 Riccardi, 2009). There are no biostratigraphically well-constrained radiometric ages for the
207 Oxfordian-Tithonian interval, while only a few $^{40}Ar/^{39}Ar$ dates from oceanic basalts are
208 retained in the current GTS2012: (*i*) 159.86 ± 3.33 (2σ) Ma and 161.17 ± 0.74 (2σ) Ma from
209 Pacific tholeiitic basalts (site 801) assigned to the Oxfordian, based on radiolarian calibration,
210 (*ii*) a revised 156.3 ± 3.4 (2σ) Ma reported for the Hawaiian basalt seafloor (site 765)
211 correlated to the base of the Kimmeridgian (P. *baylei* ammonite zone) using the M26r
212 magnetochron (Gradstein et al., 2012, Appendix 2, p. 1045), and (*iii*) an earliest Berriasian

213 $^{40}Ar/^{39}Ar$ date of 145.5 ± 0.8 (2σ) Ma from oceanic basalt sill in the Pacific Ocean (Mahoney
214 et al., 2005). Robust $^{40}Ar/^{39}Ar$ ages of 160.7 ± 0.4 (2σ) Ma and 158.7 ± 0.6 (2σ) Ma have
215 recently been obtained from two tuffs of the Lanqi Formation in north-eastern China but the
216 terrestrial fossils do not allow the attribution of a more precise stratigraphy other than a Late
217 Jurassic age (Chang et al. 2009). The only biostratigraphically well-constrained age,
218 documented by Selby (2007) on a black shale deposit from the Isle of Skye, yields a Re-Os
219 age of 154.1 ± 2.2 Ma (2σ) in the Lower Kimmeridgian just above the proposed
220 Oxfordian/Kimmeridgian GSSP.

221 As a consequence, Middle-Late Jurassic biozone duration and stage boundary ages are mainly
222 estimated by secondary radiometric guides, indirect methods and mathematical interpolations.
223 These approaches combine a magnetostratigraphic age model based on the cycle-scaling of
224 the M-sequence spreading rate model correlated to the magnetostratigraphy of outcrops (Ogg
225 et al., 2010; Przybylski et al., 2010, Gradstein et al., 2012) and cycle-derived durations of
226 ammonite zones from cycle stratigraphy (Boulila et al., 2008; 2010; Ogg et al., 2008; Huang
227 et al., 2010; Gradstein et al., 2012). Cyclostratigraphy from south-east France has
228 considerably modified ammonite biozone durations. Using a condensed section in Britain,

229 the entire Oxfordian stage had previously been fixed at 0.6 Ma, in the GTS2004. New data
230 from cyclostratigraphysuggest that the Oxfordian spanned 6.0 myr with 2 myr attributed to
231 the *Quenstedtoceras mariae* Zone alone (Boulila et al., 2008; Gradstein et al., 2012). The age
232 of the Oxfordian/Kimmeridgian boundary is now set at 157.3 ± 1.0 Ma in the GTS2012,
233 whereas it was 155.6 ± 4.0 Ma in the GTS2004 and GTS2008 (Gradstein et al. 2004; Ogg et
234 al., 2008). In this study, the $^{40}Ar/^{39}Ar$ age of 156.1 ± 0.89 Ma (2σ full uncertainty
235 propagation), attributed to the *G. transversarium* Biozone (Middle Oxfordian), is consistent
236 with the existing Re-Os age and the $^{40}Ar/^{39}Ar$ ages retained as secondary guides of the

GTS2012. Nevertheless, it falls outside of the current base and top limits of the G. *transversarium* biozone proposed respectively at 160.09 ± 1.0 Ma (2σ) and 159.44 ± 1.0 Ma (2σ), both interpolated from Oxfordian stage boundaries (Gradstein et al., 2012). The age proposed here remains compatible with the Oxfordian boundaries (163.5 ± 1.1 Ma and 157.3 ± 1.0 Ma) proposed by the GTS2012 if maximum uncertainties are taken into account. However, there is a better fit with the previous Oxfordian base (161.2±4.0 Ma) and top (155.6±4.0 Ma) from the GTS2004 and GTS2008, where the proposed boundaries were around 2 Ma younger.

The age proposed age, well constrained within the standard Jurassic biostratigraphic zonation (Cariou and Hantzpergue 1997), provides the first accurate and reliable numerical age currently available for the Late Jurassic Time Scale. This precise new tie-point can be used to anchor floating cyclostratigraphy and magnetostratigraphy, thus contributing to the improvement of seafloor spreading models, and above all, will aid in the calibration of the Late Jurassic timescale.

ACKNOWLEDGEMENTS

This work was supported by the Centre National de la Recherche Scientifique and the Commissariat à l'Energie Atomique et aux énergies alternatives. The authors thank Carmela Chateau-Smith for English proof-reading. We are grateful to J.F. Deconinck and D. Bernoulli for support and discussions about bentonites and G. Pavia and Dr G. Meléndez for help with ammonite biostratigraphy. We thank A. Coe and F. Jourdan whose constructive criticisms and detailed remarks have greatly contributed to improve the manuscript.

REFERENCES

Bernoulli, D. & Peters, T. 1970. Traces of Rhyolitic-Trachytic Volcanism in the Upper Jurassic of the Southern Alps. *Eclogae geologica Helvetica* **63/2**, 609-621.

Bonev, N. & Stampfli G. 2008. Petrology, geochemistry and geodynamic implications of Jurassic island arc magmatism as revealed by mafic volcanic rocks in the Mesozoic low-grade sequence, eastern Rhodope, Bulgaria. *Lithos* **100**, 210-233.

Boulila, S., de Rafélis, M., Hinnov, L., Gardin, S., Galbrun, B., & Collin, P. Y. 2010. Orbitally forced climate and sea-level changes in the Paleoceanic Tethyan domain (marl-limestone alternations, Lower Kimmeridgian, SE France). *Palaeogeography, Palaeoclimatology, Palaeoecology* **292**, 57-70.

Boulila, S., Hinnov, L., Huret, E., Collin, P. Y., Galbrun, B., Fortwengler, D., Marchand, D. & Thierry, J., 2008. Astronomical calibration of the Early Oxfordian (Vocontian and

Paris basins, France): consequences of revising the Late Jurassic time scale. *Earth and Planetary Science Letters* **276**, 40-51.

Cariou, E. & Hantzpergue, P. 1997. *Biostratigraphie du Jurassique oust-européen et méditerranéen: zonations parallèles et distribution des invertébrés et microfossiles*. Bulletin des Centres de Recherches Exploration – Production Elf-Aquitaine, mémoire 17, 422 pp.

Chang, S., Zhang, H., Renne, P. & Fang, Y. 2009. High-precision $^{40}Ar/^{39}Ar$ age constraints on the basal Lanqi Formation and its implications for the origin of angiosperm plants. *Earth and Planetary Science Letters* **279**, 212-221.

Channell, J. E. T., Xuan, C. & Hodell, D. A. 2009. Stacking paleointensity and oxygen isotope data for the last 1.5 Myr (PISO-1500). *Earth and Planetary Science Letters* **283**, 14-23.

Clari, P. A., Martire, L. & Pavia, G. 1990. L'unità Selcifera del Rosso Ammonitico Veronese (Alpi Meridionali). In *Atti Convegno "Fossili, Evoluzione, Ambiente": Pergola II 1987* (eds G. Pallini, et al.), pp.151-162.

Gradstein, F. M., Ogg, J. G. & Smith A. G. 2004. *A Geologic Time Scale 2004*, Cambridge University Press, 589 pp.

Gradstein, F. M., Ogg, J. G., Schmitz, M. D. & Ogg., G. M. 2012. *The Geologic Time Scale 2012*, Elsevier, 1144 pp.

Huang, C., Hesselbo, & S. P., Hinnov, L. 2010. Astrochronology of the late Jurassic Kimmeridge Clay (Dorset, England) and implications for Earth system processes. *Earth and Planetary Science Letters* **289**, 242-255.

296 Kamo, S. L. & Riccardi, A. 2009. A new U-Pb zircon age for an ash layer at the Bathonian-
297 Callovian boundary, Argentina. *GFF* **131**, 177-182.

298 Kuiper K. F., Deino A., Hilgen F. J., Krijgsman W., Renne P. R. & Wijbrans J. R. 2008.
299 Synchronizing Rock Clocks of Earth History. *Science* **320**, 500-504.

300 Mahoney, J. J., Duncan, R. A., Tejada, M. L. G., Sager, W. W., & Bralower, T. J. 2005.
301 Jurassic-Cretaceous boundary age and mid-ocean-ridge-type mantle source for Shatsky
302 Rise. *Geology* **33**, 185-188.

303 Martire, L. 1992. Sequence stratigraphy and condensed pelagic sediments. An example from
304 the Rosso Ammonitico Veronese, northeastern Italy. *Palaeogeography,*
305 *Palaeoclimatology, Palaeoecology* **94**, 169-191.

306 Martire, L. 1996. Stratigraphy, facies and sedimentary tectonics in the Jurassic Rosso
307 Ammonitico Veronese (Altopiano di Asiago, NE Italy). *Facies* **35**, 209-236.

308 Martire, L., Clari, P., Lozar, F. & Pavia G. 2006. The Rosso Ammonitico Veronese (Middle-
309 Upper Jurassic of the Trento Plateau): a proposal of lithostratigraphic ordering and
310 formalization. *Rivista Italiana di Paleontologia e Stratigrafia* **112**, 227-250.

311 Min, K. W., Mundil, R., Renne, P. R., Ludwig K.R. 2000. A test for systematic errors in Ar-
312 40/Ar-39 geochronology through comparison with U/Pb analysis of a 1.1-Ga rhyolite.
313 *Geochimica and Cosmochimica Acta* **64**, 73-98.

314 Morton, N. 2006. Chronostratigraphic units in the Jurassic and their boundaries: Definition
315 recognition and correlation, causal mechanism. *Progress in Natural Science* **16**, 1-11.

316 Nomade, S., Muttoni, G., Guillou, H., Robin, E. & Scardia, G. 2011. First $^{40}Ar/^{39}Ar$ age of the
317 Ceprano man (central Italy). *Quaternary Geochronology* **6**, 453-457.

318 Nomade, S., Gauthier, A., Guillou, H. & Pastre, J. F. 2010. $^{40}Ar/^{39}Ar$ temporal framework for
319 the Alleret maar lacustrine sequence (French Massif-Central): Volcanological and
320 paleoclimatic implications. *Quaternary Geochronology* **5**, 20-27.

321 Nomade, S., Renne, P. R., Vogel, N., Deino, A. L., Sharp, W. D., Becker, T. A., Jaouni, A. R.
322 & Mundil, R. 2005. Alder Creek sanidine (ACs-2): A Quarternary 40Ar/39Ar dating
323 standard tied to the Cobb Mountain geomagnetic event. *Chemical Geology* **218**, 315-338.

324 Ogg, J. G., Coe, A. L., Przybylski, P. A. & Wright, J. K. 2010. Oxfordian
325 magnetostratigraphy of Britain and its correlation to Tethyan regions and Pacific marine
326 magnetic anomalies. *Earth and Planetary Science Letters* **289**, 433-448.

327 Ogg, J. G., Ogg G. & Gradstein, F. M. 2008. *The concise Geological Time Scale*. Cambridge
328 University Press, 177 pp.

329 Ogg, J. G. & Smith, A.G., 2004. The geomagnetic polarity time scale. In *A Geological Time*
330 *Scale 2004* (eds F. M. Gradstein, J. G. Ogg, & A. Smith), pp.63-86. Cambridge
331 University Press.

332 Pálfy J. 2008. The quest for refined calibration of the Jurassic time-scale. *Proceedings of the*
333 *Geologists' Association* **119**, 85–95.

334 Pearce, J. A. (1982). Trace element characteristics of lavas from destructive plate boundaries.
335 In: *Andesites. Orogenic Andesites and Related Rocks* (ed. R. S. Thorpe), pp. 525–549.
336 Wiley, Chichester.

337 Pellenard, P. & Deconinck, J. F. 2006. Mineralogical variability of Callovo-Oxfordian clays
338 from the Paris Basin and the Subalpine Basin. *Comptes Rendus Geoscience* **338**, 854-866.

339 Pellenard, P., Deconinck, J. F., Huff, W., Thierry, J., Marchand, D., Fortwengler, D. &
340 Trouiller, A. 2003. Characterization and correlation of Upper Jurassic (Oxfordian)
341 bentonite deposits in the Paris Basin and the Subalpine Basin, France. *Sedimentology* **50**,
342 1035-1060.

343 Przybylski, P. A., Ogg. J. G., Wierzbowski, A., Coe, A. L., Hounslow, M. W., Wright, J. K.,
344 Atrops, F. & Settles, E. 2010. Magnetostratigraphic correlation of the Oxfordian-
345 Kimmeridgian boundary. *Earth and Planetary Science Letters* **289**, 256-272.

346 Renne, P. R., Mundil, R., Balco, G., Min, K. & Mudwig, K.R. 2010. Joint determination of
347 ^{40}K decay constants of ^{40}K decay constants and ^{40}Ar/^{40}K for the Fish Canyon sanidine
348 standard, and improved accuracy for Ar-40/Ar-39 geochronology. *Geochimica et*
349 *Cosmochimica Acta* **74**, 5349-5367.

350 Renne, P. R., Mundil, R., Balco, G., Min, K. & Mudwig, K. R. 2011. Response to the
351 comment by W. H. Schwarz et al. on "Joint determination of ^{40}K decay constants and
352 ^{40}Ar*/^{40}K for the Fish Canyon sanidine standard, and improved accuracy for ^{40}Ar/^{39}Ar
353 geochronology" by P.R. Renne et al. (2010). *Geochimica et Cosmochimica Acta* **75**,
354 5097-5100.

355 Sarti, C. 1985. Biostratigraphie et faune à ammonites du Jurassique supérieur de la plate-
356 forme atesine (Formation du Rosso Ammonitico Veronais). *Revue de Paléobiologie* **4**,
357 321-330.

358 Sarti, C. 1993. Il Kimmeridgiano delle Prealpi Veneto-Trentine : fauna e biostratigrafia, *Mem.*
359 *Museo Civico Storia Nat. Verona* **5**, 9-144.

360 Selby, D. 2007. Direct Rhenium-Osmium age of the Oxfordian-Kimmeridgian boundary,
361 Staffin bay, Isle of Skye, U.K., and the Late Jurassic time scale. *Norwegian Journal of*
362 *Geology* **47**, 291-299.

363 Spears, D. A., Kanaris-Sotiriou, R., Riley, N. & Krause, P. 1999. Namurian bentonites in the
364 Pennine Basin, UK – origin and magmatic affinities. *Sedimentology* **46**, 385–401.

365 Steiger, R. H. & Jäger, E. 1977. Subcommission on geochronology: convention on the use of
366 decay constants in geo-and cosmochronology. *Earth and Planetary Science Letters* **36**,
367 359-362.

368 Thorpe, R. S., Francis, P. W. & O'Callaghan, L. 1984. Relative roles of source composition,
369 fractional crystallization and crustal contamination in the petrogenesis of Andean
370 volcanic rocks. *Phil. Trans. R. Soc. London* **310**, 675–682.
371

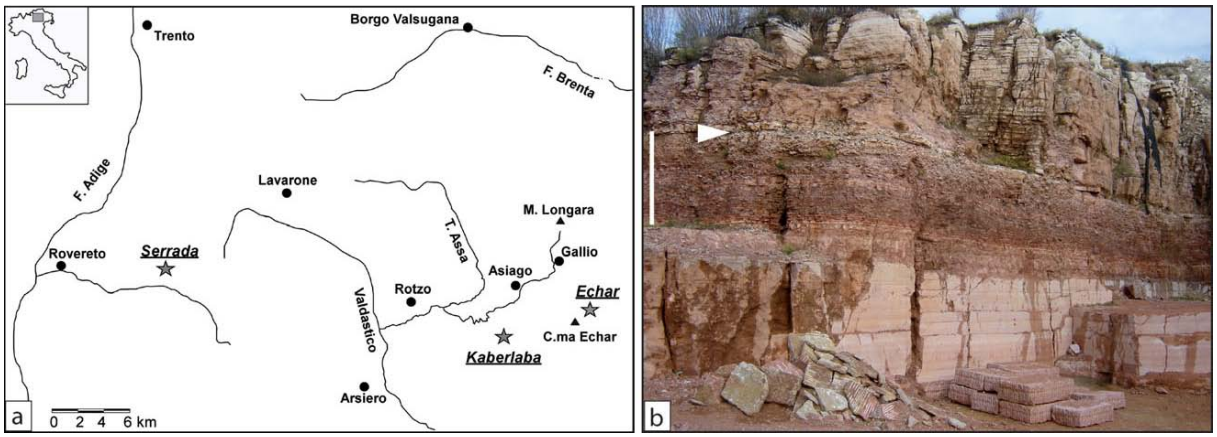

Figure 1. (a) Locality map of the sections sampled in the Altopiano di Asiago region : Kaberlaba (45°50'27.38"N ; 11°29'47.56"E), Echar (45°51'21.24"N ;11°34'44.47"E) and Serrada (45°53'16.10"N ; 11°09'12.40"E); (b) view of the 3 members of the RAV in the Kaberlaba quarry. Scale bar corresponds to 5.2 m, the thickness of the middle unit (RAM). The RAM unit contains typical chert layers and several bentonite layers. The position of the thickest bentonite AB4 is indicated (white arrow).

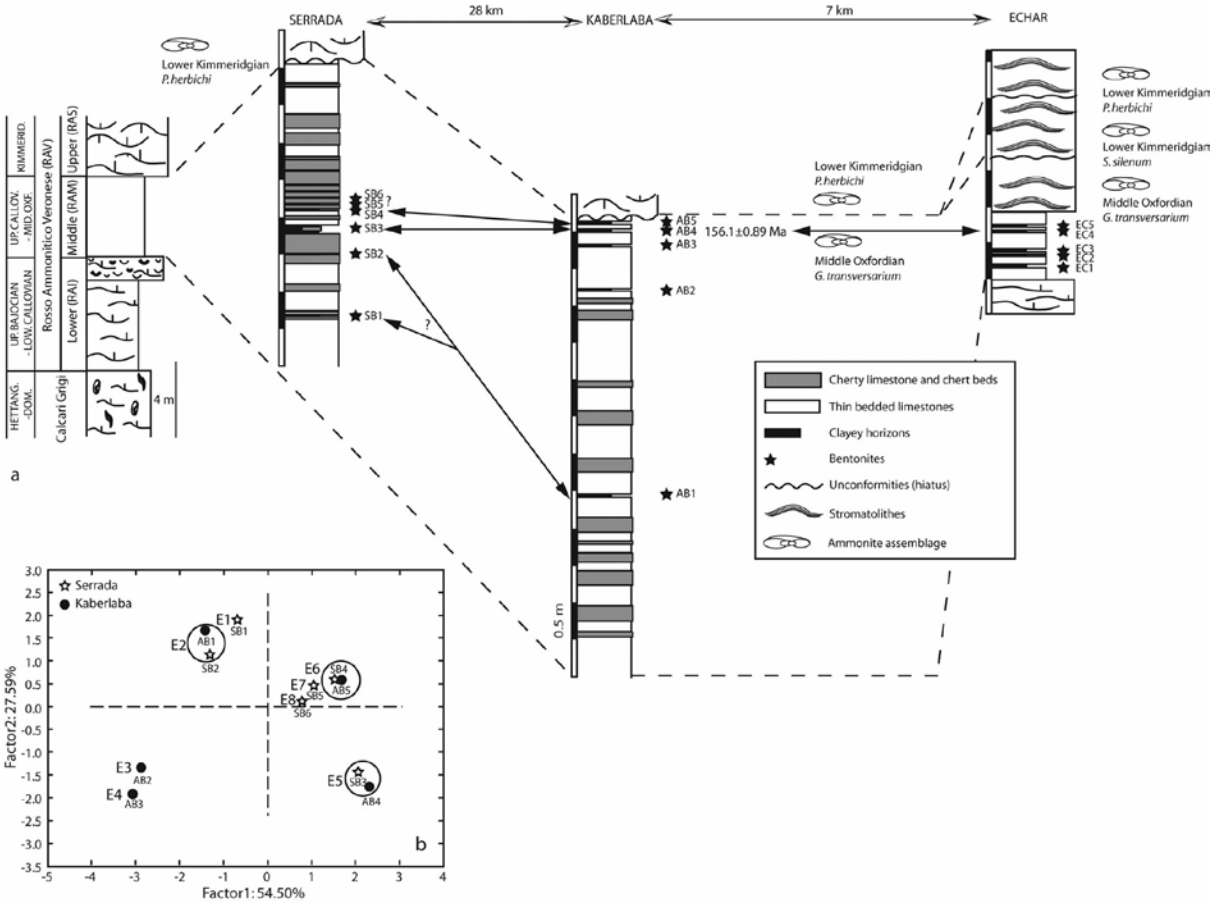

Figure 2. (a) Detailed logs of the three sections measured, showing correlations between bentonite layers and the $^{40}Ar/^{39}Ar$ dated AB4 bentonite (Kaberlaba), attributed to the G. *transversarium* Biozone. (b) PCA based on Al_2O_3-normalised Hf, Ga, Th, Ta, La, Zr and Ti concentrations. Circles correspond to proposed correlations between bentonite layers. E1 to E8 number the volcanic events.

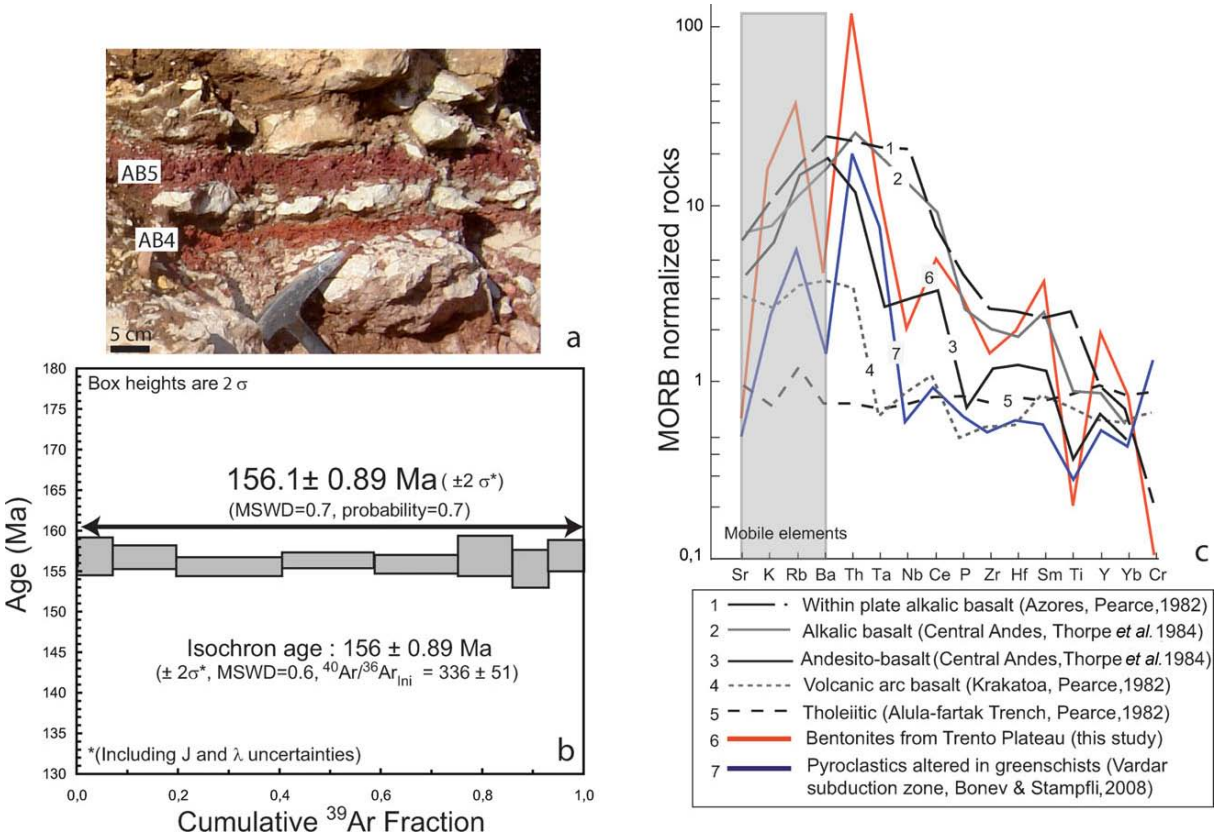

Figure 3. (a) Photograph of AB4 and AB5 bentonites intercalated between nodular limestones of the RAM unit (Middle Oxfordian) and overlain by the unconformity between the RAM and RAS units. (b) Apparent age spectra for AB4, showing a well-defined plateau age of 156.1 ± 0,89 Ma (2σ external). (c) MORB-normalised multi-element diagram for bentonite layers, pyroclastic deposits from the Vardar domain and comparative patterns for standard rocks from various geodynamic contexts.

401

402

K Total decay Constant	Steiger & Jäger (1977)	Steiger & Jäger (1977)	Renne et al., (2011)
Standard used	ACs (1.194 Ma) (1)	ACs (1.201 Ma) (2)	ACs (1.206 Ma) (3)
Equivalent FCs age	28.02 Ma	28.20 Ma	28.29 Ma
Age (Ma)	154.6	155.6	156.1
2σ (Ma)*	4.0	4.0	1.8

403 Table 1

404

405 **Table 1**: Calculated ages and corresponding uncertainties using various total K decay
406 constants. *The uncertainty reported is the full propagated uncertainty. (1): Nomade et al.,
407 2003; (2): Kuiper et al., 2008; (3): Renne et al., 2011. Alder Creek sanidine; FCs – Fish Creek
408 sanidine.

409